Journal of Computational Physics 229 (2010) 6663–6672

Contents lists available at ScienceDirect

Journal of Computational Physics

journal homepage: www.elsevier.com/locate/jcp

Short note

A volume of fluid approach for crystal growth simulation

J. López [a], P. Gómez [b], J. Hernández [b,*]

[a] Dept. de Ingeniería de Materiales y Fabricación, ETSII, Universidad Politécnica de Cartagena, E-30202 Cartagena, Spain
[b] Dept. de Mecánica, ETSII, UNED, E-28040 Madrid, Spain

ARTICLE INFO

Article history:
Received 24 July 2009
Received in revised form 21 May 2010
Accepted 25 May 2010
Available online 2 June 2010

Keywords:
Volume of fluid method
Distance function
Solidification
Dendritic growth simulation

ABSTRACT

A new approach to simulating the dendritic growth of pure metals, based on a recent volume of fluid (VOF) method with PLIC (piecewise linear interface calculation) reconstruction of the interface, is presented. The energy equation is solved using a diffuse-interface method, which avoids the need to apply the thermal boundary conditions directly at the solid front. The thermal gradients at both sides of the interface, which are needed to obtain the front velocity, are calculated with the aid of a distance function to the reconstructed interface. The advection equation of a discretized solid fraction function is solved using the unsplit VOF advection method proposed by López et al. [J. Comput. Phys. 195 (2004) 718–742] (extended to three dimensions by Hernández et al. [Int. J. Numer. Methods Fluids 58 (2008) 897–921]), and the interface curvature is computed using an improved height function technique, which provides second-order accuracy. The proposed methodology is assessed by comparing the numerical results with analytical solutions and with results obtained by different authors for the formation of complex dendritic structures in two and three dimensions.

1. Introduction

Although the volume of fluid (VOF) method is one of the most widely used methods for simulating interfacial flows with fixed grids (see, for example, [25]), its application to phase change processes in solidification problems is not common. The interface curvature computation and the need for an adequate estimation of the interfacial jump conditions, which usually involve a discontinuity in the thermal gradient at the solid front, impose severe requirements on the methods used to study the formation of microstructure during solidification. Among the methods most frequently used to simulate the growth of dendrites in solidification problems, we can mention the front-tracking method [13], in which the energy equation is solved using a fixed grid and the interface is explicitly tracked using a set of marker points (there are several examples of two-dimensional [30,35,3,36] and three-dimensional [4,37] applications); the phase-field method, which uses an auxiliary variable that varies smoothly from zero to unity over a diffuse-interface region between the two phases (see, for example, [32,23,14,5], and the review in [6]), and the level-set method, in which the interface is embedded as the zero-level set of a higher-dimensional function, usually a signed distance function (see, for example, [26,8,15,10]). Jacot and Rappaz [12] proposed a two-dimensional method, referred to by these authors as a pseudo front-tracking method, which calculates a distance function to a PLIC (piecewise linear interface calculation) reconstructed interface, from which the interface curvature is calculated. Another approach which has certain similarities with VOF methods is the enthalpy method, although the interface evolution is not directly derived from the solution of the solid fraction advection equation [28,22,31].

In this work we present a new approach to the simulation of dendritic growth of pure metals, based on a VOF method with PLIC reconstruction of the interface. To the best of our knowledge, this is the first time that a numerical procedure that

* Corresponding author. Tel.: +34 91 398 6424; fax: +34 91 398 6536.
E-mail addresses: joaquin.lopez@upct.es (J. López), pgomez@ind.uned.es (P. Gómez), jhernandez@ind.uned.es (J. Hernández).

0021-9991/$ - see front matter © 2010 Elsevier Inc. All rights reserved.
doi:10.1016/j.jcp.2010.05.026

essentially relies on a VOF-type method has been used to simulate dendritic growth. To solve the energy equation, we use, as many authors have, a diffuse-interface method which avoids the need of applying the thermal boundary conditions directly at the liquid/solid front. Our formulation is similar to that used by Juric and Tryggvason [13] or Zabaras and Samanta [34], among others, in which the liberation or absorption of latent heat at the diffuse-interface is taken into account as a source term in the energy equation. The thermal gradients at both sides of the interface, which are needed to accurately obtain the front velocity, are calculated with the aid of a distance function. The distance function is obtained at every time step by computing the exact distances from the computational cells surrounding the interface to the reconstructed interface segments (polygons in 3D). The advection equation of a discretized solid fraction function, which is equal to one in solid cells, zero in liquid cells and has a value between zero and one in interfacial cells, is solved using the unsplit VOF advection method proposed by López et al. [16] (extended to three dimensions by Hernández et al. [11]). The height function (HF) technique, which is a good alternative to compute interface curvatures from volume fractions (see, for example, Refs. [9,20]), and in particular the improved HF technique proposed by López et al. [19], is used in this work. The accuracy and efficiency of the proposed methodology are assessed by comparing the numerical results with analytical solutions and with results obtained by different authors for the formation of complex dendritic structures in two and three dimensions.

2. Numerical model

The solidification of a pure metal is considered, assuming that the thermo-physical and transport properties of both phases are constant. The interface evolution is described with the aid of a VOF-PLIC method for the advection and reconstruction of the liquid/solid interface, which will be presented in Section 2.1. A volume-averaging approach is followed to solve the energy equation, assuming that the solidification process occurs in a zone of finite thickness around the reconstructed interface, as described in Section 2.2. A distance function, constructed as indicated in Section 2.3, is used to obtain the thermal gradients at both sides of the interface, as described in Section 2.4.

2.1. Interface tracking

The interface is evolved from every instant t^n to t^{n+1} using a PLIC-VOF approach. The interface is first reconstructed in each interfacial cell using Youngs' PLIC scheme (implemented as indicated in [17]), and then advected to the next time step using the evolution equation for the solid volume fraction, f, which is continuous everywhere except at the interface, where it jumps from zero to one:

$$\frac{\partial f}{\partial t} + \boldsymbol{v}\cdot\nabla f = 0, \tag{1}$$

which can be rewritten as

$$\frac{\partial f}{\partial t} + \nabla\cdot(\boldsymbol{v}f) - f\nabla\cdot\boldsymbol{v} = 0, \tag{2}$$

where the velocity vector field used will be defined in Section 2.4.1.

Integrating over a given cell, Ω, of volume V_Ω, and the time interval $\Delta t = t^{n+1} - t^n$, the following expression is obtained at each time step for the volume fraction of the solid phase in the cell, F, which is the discretized version of the function f:

$$F^{n+1} = F^n - \frac{1}{V_\Omega}\int_{t^n}^{t^{n+1}}\int_\Omega \nabla\cdot(\boldsymbol{v}f)\mathrm{d}\Omega\mathrm{d}t + \frac{1}{V_\Omega}\int_{t^n}^{t^{n+1}}\int_\Omega f\nabla\cdot\boldsymbol{v}\mathrm{d}\Omega\mathrm{d}t. \tag{3}$$

The first integral in Eq. (3), which represents the net volume fraction advected out of the cell, V_{F_T}, will be solved geometrically using the unsplit advection method proposed by López et al. [16] (extended to 3D by Hernández et al. [11]). The second integral in Eq. (3) represents the variation in the volume of the solid phase in the cell due to phase change. Using a semi-implicit method to calculate this integral, Eq. (3) is expressed as

$$F^{n+1} = \left[F^n\left(1+\frac{1}{2}\nabla\cdot\boldsymbol{v}^{n+1/2}\Delta t\right) - \frac{V_{F_T}}{V_\Omega}\right] \Big/ \left(1-\frac{1}{2}\nabla\cdot\boldsymbol{v}^{n+1/2}\Delta t\right), \tag{4}$$

where the term $\nabla\cdot\boldsymbol{v}^{n+1/2}$ is discretized at the cell center using a standard second-order finite difference approximation and assuming $\boldsymbol{v}^{n+1/2} = \frac{3}{2}\boldsymbol{v}^n - \frac{1}{2}\boldsymbol{v}^{n-1}$. Note that an explicit computation of the second integral in Eq. (3) yields the following expression:

$$F^{n+1} = F^n(1+\nabla\cdot\boldsymbol{v}^n\Delta t) - \frac{V_{F_T}}{V_\Omega}. \tag{5}$$

The merits of using Eq. (4) instead of Eq. (5) are discussed in Section 3.1.1. Note that, despite the semi-implicit discretization in time of Eq. (3), the geometrical procedure used to calculate fluxes through the cell faces does not allow CFL values greater than 1 to be used.

The final volume fraction distribution at time t^{n+1} is obtained imposing the following limiting conditions:

$$F^{n+1,\text{update}} = \begin{cases} \min[1.0, \max(F^n, F^{n+1})] & \text{if } V^{n+1/2} \geqslant 0, \\ \max[0.0, \min(F^n, F^{n+1})] & \text{if } V^{n+1/2} < 0, \end{cases} \tag{6}$$

where V is the interface velocity, which is calculated as indicated in Section 2.4.1. Eqs. (4) and (6) constitute the key point of the advection procedure. Note that a positive interface velocity means that the front advances from the solid to the liquid phase (solidification process), and therefore the value of F cannot decrease. A similar comment can be made when the value of V is negative (melting process). The above conditions avoid the formation of 'undershoots' (values of F lower than 0.0) or 'overshoots' (values of F higher than 1.0). It also avoids, for example, the partial melting of a cell completely solidified (that is, with $F^n = 1$), in which $V > 0$, due to integration inaccuracies of the volume fraction evolution equation. These inaccuracies, however, may still produce the artificial generation of "wisps"; i.e., small volumes of liquid in solid regions or of solid in liquid regions, which in the present work have been simply eliminated (as an example, in the test cases of Section 3.2.1, using a grid of 400^2 cells, the "wisp" volumes are generally lower than about a 10^{-3}% of the total solid volume).

2.2. Energy equation

As already mentioned, it will be assumed that solidification occurs in a zone of finite thickness around the reconstructed liquid/solid interface. Following a volume-averaging approach [34,13], the energy equation can be expressed as

$$\rho c \frac{\partial T}{\partial t} = \nabla \cdot (k \nabla T) - \mathcal{Q}\dot{\Phi} \tag{7}$$

with

$$\Phi = \begin{cases} 0, & \text{if } \phi < -\epsilon, \\ 1, & \text{if } \phi > \epsilon, \\ 0.5 + \phi/2\epsilon, & \text{if } -\epsilon \leqslant \phi \leqslant \epsilon, \end{cases}$$

where $\mathcal{Q} = \rho_+[L + (c_+ - c_-)(T_I - T_m)]$ (see Ref. [1]); ϵ is the half-thickness of the diffuse liquid/solid interface; ϕ is a distance function to the reconstructed interface, which is computed as described in Section 2.3; $\dot{\Phi}$ is the local time derivative of Φ; L is the latent heat of solidification; T_m is the pure material melting temperature; T_I is the interface temperature, and subscripts $-$ and $+$ denote liquid and solid phases, respectively. The density, thermal conductivity and heat capacity in each computational cell are calculated, respectively, from

$$\rho = \rho_- + (\rho_+ - \rho_-)F, \quad k = k_- + (k_+ - k_-)F, \quad c = c_- + (c_+ - c_-)F.$$

The last term of Eq. (7) is a source term which accounts for the latent heat released (absorbed) during solidification (melting) at the diffuse liquid/solid interface. In this work, ϵ is taken to be equal to the size of the computational cell, h. It has been observed that this choice may affect the results in some cases, but the above mentioned value was found to provide the best overall performance for the tests carried out in the present work.

Eq. (7) is discretized using central differences for the spatial derivatives and a fully implicit time integration scheme. A uniform Cartesian computational grid is used, in which the discrete values of the temperature, distance function and material properties are stored at cell centers. The system of linear equations that arise from the discretization of Eq. (7) has been solved using a preconditioned bi-conjugate gradient stabilized (Bi-CGSTAB) method with an incomplete LU factorization preconditioning matrix [24].

2.3. Distance function construction

Once the interface is reconstructed in every interfacial cell as a plane defined by $\boldsymbol{n}\cdot\boldsymbol{x} + C = 0$ using a PLIC scheme, where $\boldsymbol{n}$ points to the solid, the distance between the center of a computational cell and the interface (defined by all the polygons resulting from the intersection between the interfacial cells and the corresponding interface planes) is computed as follows:

1. In every cell of the domain with center at coordinates (l,m,n), the signed distance function is initialized as follows:

$$\phi_{l,m,n} = \begin{cases} \phi_0 & \text{if } F_{l,m,n} \geqslant 0.5, \\ -\phi_0 & \text{if } F_{l,m,n} < 0.5, \end{cases} \tag{8}$$

where $F_{l,m,n}$ is the solid volume fraction of the cell. The initial value ϕ_0 is made equal to $3h$.

2. The distance, d, to the interface polygon of every interfacial cell with center at (l',m',n') $(0 < F_{l',m',n'} < 1)$ is computed from every cell (l,m,n) satisfying the condition

$$(l-l')^2 + (m-m')^2 + (n-n')^2 \leqslant 4^2. \tag{9}$$

The distance function $\phi_{l,m,n}$ is then updated as

$$\phi_{l,m,n} = \text{sign}(\phi_{l,m,n}) \min(d, |\phi_{l,m,n}|). \tag{10}$$

3. For every cell (l',m',n') with $F_{l',m',n'}$ equal to 1.0 or 0.0 and which has an adjacent cell with a volume fraction equal to 0.0 or 1.0, respectively, the shortest distance d to the cell boundaries (cell faces, cell edges or corners) is computed from every cell (l,m,n) satisfying the condition of Eq. (9) and $\text{sign}(\phi_{l,m,n})\text{sign}(\phi_{l',m',n'}) < 0$. The distance function $\phi_{l,m,n}$ is then updated using Eq. (10).

Note that, in order to reduce the CPU-time consumed by the algorithm, the distance function is calculated only in a local region around the interface, which in this work is taken to be of thickness $6h$. The source code and pseudo-code for the algorithms used to obtain the interface polygon at every interfacial cell [18] and to compute the distance from a cell center to an interface polygon are available for download at [38]. Sussman and Puckett [27], Bourlioux [7], Menard et al. [21] and Yang et al. [33] proposed similar algorithms to compute the distance from a point to an interface polygon, although they did not provide implementation details.

2.4. Computation of interface quantities

2.4.1. Interface velocity

The velocity of the solidification front, V, is determined from the energy balance at the interface, given by

$$V = \frac{[q]}{\mathcal{Q}}, \tag{11}$$

where $[q] = q_+ - q_-$ is the jump in heat flux through the interface, which is calculated as indicated below in Section 2.4.2. The velocity V is computed in what we will call interfacial nodes (in), which include the centers of the interfacial cells (ic), where $0 < F < 1$, and the centers of cells (adj) adjacent to the former (with one face in common), which satisfy the condition $\phi_{ic}\phi_{adj} \leqslant 0$ (see Fig. 1(a)). Finally, the interface velocity is extended away from the interface over a narrow band of thickness $6h$, using the method proposed by Tan and Zabaras [29]. This thickness is the minimum size of the region where the velocity must be defined to solve the VOF advection equation. The extended velocity, V_{ext}, provides the velocity vector field used in Section 2.1 to advance the interface to the next time step,

$$\boldsymbol{v} = -\frac{\nabla\phi}{|\nabla\phi|}V_{ext}.$$

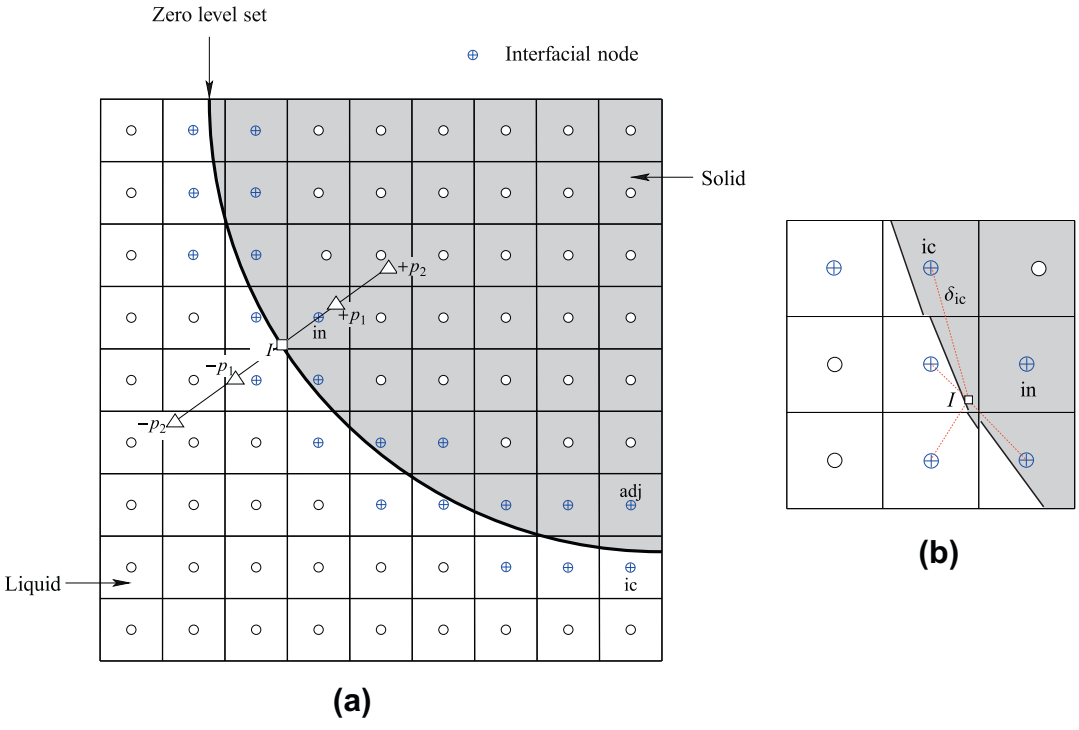

Fig. 1. (a) Interfacial nodes: centers of interfacial cells (ic), where $0 < F < 1$, and centers of adjacent cells (adj) having one edge in common with any interfacial cell and satisfying the condition $\phi_{ic}\phi_{adj} \leqslant 0$. (b) Interfacial cells involved in interface curvature calculation at $\boldsymbol{x}_I$.

2.4.2. Heat flux jump

For each interfacial node (in), the heat fluxes at the liquid and solid sides of the interface, q_- and q_+, respectively, are calculated at the closest point located in the zero-level set (point I in the 2D example of Fig. 1(a)), following a procedure similar to that used in [30]. The location of point I is obtained as

$$\boldsymbol{x}_I = \boldsymbol{x}_{\text{in}} - \boldsymbol{n}_{\text{in}}\phi_{\text{in}}, \tag{12}$$

where $\boldsymbol{n}_{\text{in}} = (\nabla\phi/|\nabla\phi|)_{\text{in}}$ is computed using central differences. Then, two probe points at each side of the interface are defined as

$$\boldsymbol{x}_{\pm p_1} = \boldsymbol{x}_I \pm h\boldsymbol{n}_{\text{in}}, \tag{13}$$
$$\boldsymbol{x}_{\pm p_2} = \boldsymbol{x}_I \pm 2h\boldsymbol{n}_{\text{in}} \tag{14}$$

and the heat fluxes are calculated as

$$q_\pm = \pm k_\pm \frac{1.5T_I - 2T_{\pm p_1} + 0.5T_{\pm p_2}}{h}, \tag{15}$$

where temperatures $T_{\pm p_1}$ and $T_{\pm p_2}$ are obtained using trilinear interpolations, and the interface temperature, T_I, may in general be a function of the interface curvature and velocity.

2.4.3. Interface curvature

The interface curvature, which may be involved in the calculation of the liquid/solid interface temperature, as in the tests presented in Section 3, is obtained at $\boldsymbol{x}_I$ from the weighted interpolation

$$\kappa = \frac{\sum_{\text{ic}} \kappa_{\text{ic}}/\delta_{\text{ic}}}{\sum_{\text{ic}} 1/\delta_{\text{ic}}},$$

where κ_{ic} is computed using the improved HF technique proposed by López et al. [19], δ_{ic} is the distance from point I to the center of the interfacial cell ic (Fig. 1(b)) and the summation extends over the cell containing point I (provided that, as generally occurs, this cell is an interfacial cell, where $0 < F < 1$) and the interfacial cells adjacent to this one.

3. Results and discussion

All the simulations carried out in this section involving the solution of Eq. (7) have been made using the same thermophysical and transport properties for the solid and liquid regions ($c_+ = c_- = 1$, $k_+ = k_- = 1$ and $\rho_+ = \rho_- = 1$) and $L = 1$.

3.1. Problems with analytical solutions

3.1.1. Tests with prescribed velocity field

The solid region is initially a circle (sphere in 3D) of radius unity, which is expanded in a uniform radial velocity field equal to 1 (note that the extension of the velocity outward from the interface is not necessary). Table 1 shows the error $E = |R(t=1) - 2|$, where $R(t=1)$ is the mean radius of the interface at $t = 1$, obtained as $\left(\sum_{i,j,k} F/\pi\right)^{1/2} h$ in 2D and as $\left(\sum_{i,j,k} 3F/4\pi\right)^{1/3} h$ in 3D, and order of convergence, $\mathcal{O}$, obtained using a time step $\Delta t = 0.1h$, different grid sizes and Eqs. (4) and (5) to advect the volume fraction distribution. It can be observed that a considerable improvement can be obtained, either in two or three dimensions, when a semi-implicit scheme is used to solve the advection equation for the solid fraction. Note that the semi-implicit scheme provides second-order convergence and reduces the errors by almost one order of magnitude with respect to the explicit scheme for the finest grid considered.

Table 1
Error and order of convergence obtained in the tests of circle and sphere expansion with a prescribed radial velocity equal to 1.

Grid size, h	Circle				Sphere			
	Using Eq. (5) (explicit)		Using Eq. (4) (semi-implicit)		Using Eq. (5) (explicit)		Using Eq. (4) (semi-implicit)	
	E	$\mathcal{O}$	E	$\mathcal{O}$	E	$\mathcal{O}$	E	$\mathcal{O}$
10/32	1.91×10^{-2}		8.41×10^{-3}		3.54×10^{-2}		1.42×10^{-2}	
		1.4		2.1		1.3		2.0
10/64	7.39×10^{-3}		2.03×10^{-3}		1.42×10^{-2}		3.49×10^{-3}	
		1.2		2.0		1.2		2.0
10/128	3.18×10^{-3}		5.07×10^{-4}		6.25×10^{-3}		8.65×10^{-4}	

3.1.2. Frank sphere test

In this test, taken from the work of Chen et al. [8], the solid region is a circle of radius R centered in the domain, and the temperature field in parametric form is given by

$$T(r,t) = T(s) = \begin{cases} T_\infty\left(1 - \frac{F(s)}{F(S)}\right) & \text{for } s > S \\ 0 & \text{for } s \leqslant S, \end{cases} \tag{16}$$

where T_∞ is a given undercooling, r is the distance to the center of the domain, $s = r/t^{1/2}$, $S = R/t^{1/2}$, and $F(s) = \int_{s^2/4}^{\infty} e^{-z}/z dz$. An exact solution in two dimensions can be found in [2]. The results for the mean radius evolution obtained for $T_\infty = -0.5$, a domain of size 16×16, homogeneous Neumann boundary conditions (insulated domain), different grid sizes and a time step $\Delta t = 0.1h$ are presented in Fig. 2(a). It can be observed that the computed results for fine grids are very close to the exact solution. The results compare favorably with those presented by Chen et al. [8] in their Fig. 5 and Gibou et al. [10] in their Fig. 7. The error between the exact and computed mean radius is represented in Fig. 2(b) as a function of grid size at the instant $t = 1.5$, showing second-order convergence.

3.2. Dendritic growth simulations

3.2.1. 2D tests

The first test presented in this section is that proposed by Juric and Tryggvason [13], in which the following Gibbs–Thomson relation is considered for the interface temperature:

$$T_I = \epsilon_\kappa \kappa - \epsilon_V V, \tag{17}$$

where $\epsilon_\kappa = \epsilon_V = 0.002$ (in the present work, κ is negative when the center of curvature lies in the solid phase). Note that surface tension and interface kinetic effects in stable solidification are negligible, and are only accounted for when the Gibbs–Thomson effect is significant, as in the cases of unstable solidification that are included in this section. An initial solid seed, given in parametric form by

$$\begin{aligned} x(s) &= [0.1 + 0.02\cos(8\pi s)]\cos(2\pi s) \\ y(s) &= [0.1 + 0.02\cos(8\pi s)]\sin(2\pi s) \end{aligned} \tag{18}$$

is considered in the center of a domain of size 4×4 with all the boundaries insulated. The initial temperatures of the solid seed and of the undercooled region are made equal to 0.0 and -0.5, respectively. The time step has been chosen as $\Delta t = 0.05h/V_{\max}$, where $V_{\max}$ is the maximum Cartesian component of $\boldsymbol{v}$.

A simple iterative procedure is used to solve the coupling between Eqs. (17), (11) and (15) until the difference between the interface temperatures of two consecutive iteration steps at any cell of the domain is lower than 10^{-8} (for the finest grid used, the solution generally converges in 10 or less iterations).

Fig. 3 shows the results of the test for the evolution of the interface shape, in time increments of 0.04 up to $t = 1.0$, obtained with three different grid sizes. As mentioned by Tan and Zabaras [29], this problem is non-trivial and highly sensitive to perturbations during the solidification process, which makes it difficult to obtain grid independence (substantial differences in published results can be found in [13,35,8,36,29]). In this work, almost grid-independent results have been obtained

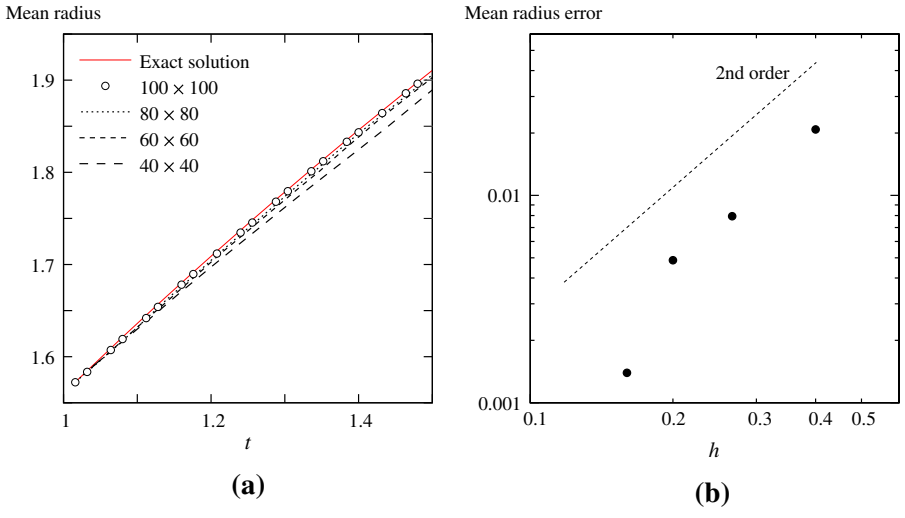

Fig. 2. Frank sphere test. (a) Mean radius as a function of time for different grid sizes. (b) Mean radius error as a function of grid size at the instant $t = 1.5$.

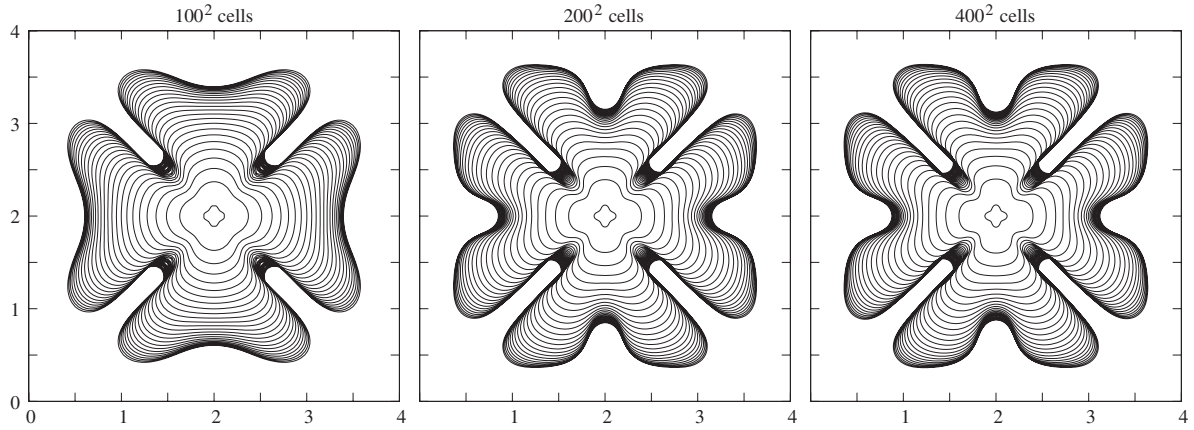

Fig. 3. Results of the dendritic growth simulation test in 2D obtained with three different grid sizes and $\epsilon_\kappa = \epsilon_V = 0.002$.

for the intermediate grid used, and a very good agreement with the results presented by Udaykumar et al. [30] and Zhao and Heinrich [36] has been found. The grid independence obtained for this unstable problem can be more clearly observed in Fig. 4, which shows the superimposed interface shapes obtained using different grid sizes. A visual comparison with the results presented in [30,36] shows a very good agreement with the most accurate of the results obtained by these authors using a front-tracking method.

To evaluate the effect of grid anisotropy on the results, the same initial seed (Fig. 5(a)) was rotated 19° and 45° with respect to grid lines (Fig. 5(b) and (c), respectively). In order to avoid boundary effects, the simulations were stopped at the instant $t = 0.14$. It can be observed from Fig. 5(d), where the results of all the simulations are rotated to 0° and superimposed, that the interface shapes are almost coincident (similar results were also obtained by Zhao and Heinrich [35]).

Steady-state results obtained for dendritic growth with the proposed model were compared with the predictions of the microscopic solvability theory. For this purpose, we carried out a test taken from [15], in which it is assumed that, in Eq. (17), $\epsilon_\kappa = 0.5(1 - 0.75\cos 4\theta)$, where θ is the angle between the outward interface normal vector and the x-direction, and $\epsilon_V = 0$. An initial circular solid seed of radius 15 is considered in the center of a domain of size 800×800 with all the boundaries insulated. The initial temperatures of the solid seed and of the undercooled region are made equal to 0.0 and -0.55, respectively. A grid of 1000×1000 cells and a time step of $\Delta t = 0.05h/V_{\max}$ were used in the simulation. The results obtained for the interface velocity at the dendrite tips as a function of time differ by less than 1.4% from those obtained in [15] using a phase-field method, the difference being smaller than a 0.5% at $t = 5000$. In a simulation made in a larger domain of size 1200×1200 (which ensured keeping the dendrite tips far from the domain boundaries), the interface velocity at the dendrite tips obtained at $t = 9000$ was 0.035, which is in good agreement with the steady-state value of 0.034 predicted by the microscopic solvability theory [15]. A similar degree of agreement was obtained for an undercooling of -0.65.

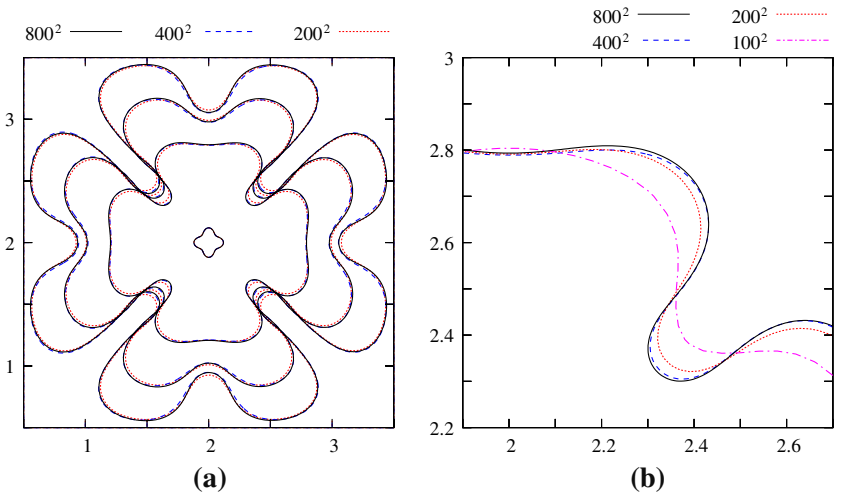

Fig. 4. Dendritic growth simulation test in 2D; same conditions as in Fig. 3. (a) Superimposed results for the interface shape obtained with three different grid sizes at various instants, in time increments of 0.2. (b) Detail of the superimposed interfaces obtained with four different grid sizes at $t = 0.2$.

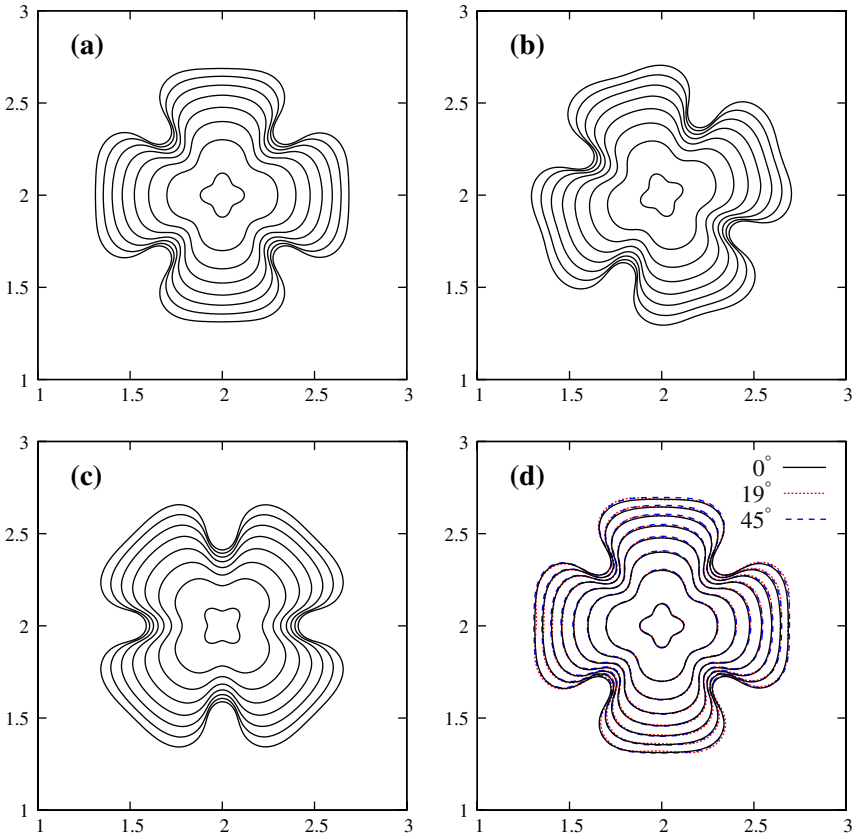

Fig. 5. Dendritic growth simulation test in 2D; same conditions as in Fig. 3. Results for the interface shape in time increments of 0.02, obtained using a 400^2 grid and an initial solid seed with different orientations with respect to grid lines. (a) 0°; (b) 19°; (c) 45° and (d) rotated and superimposed interface shape results of cases (a)–(c).

3.2.2. 3D test

In order to assess the performance of the proposed model in the simulation of dendritic growth in 3D, a test taken from [37,4] is considered. The interface temperature is assumed to be given by $T_I = 1 \times 10^{-4}\left\{1 - 0.3\left[4\left(n_x^4 + n_y^4 + n_z^4\right) - 3\right]\right\}\kappa$, where (n_x,n_y,n_z) are the components of the interface normal vector $\boldsymbol{n}$, calculated as $\nabla\phi/|\nabla\phi|$ at the corresponding interfacial node using central differences. The initial seed is a sphere of radius $R_0 = 0.035$ perturbed as $R = R_0\{1 + 0.1\cos[\alpha\pi/\arccos(1/\sqrt{3})]\}$, where $\alpha = \arccos(\max(|n_x|,|n_y|,|n_z|))$. An octant, of size 0.5^3, of the domain is considered, with appropriate boundary conditions applied at the symmetry planes. The initial temperatures of the solid seed and of the undercooled region are made equal to 0.0 and -0.15, respectively. The time step is chosen as $\Delta t = 0.05h/V_{\max}$.

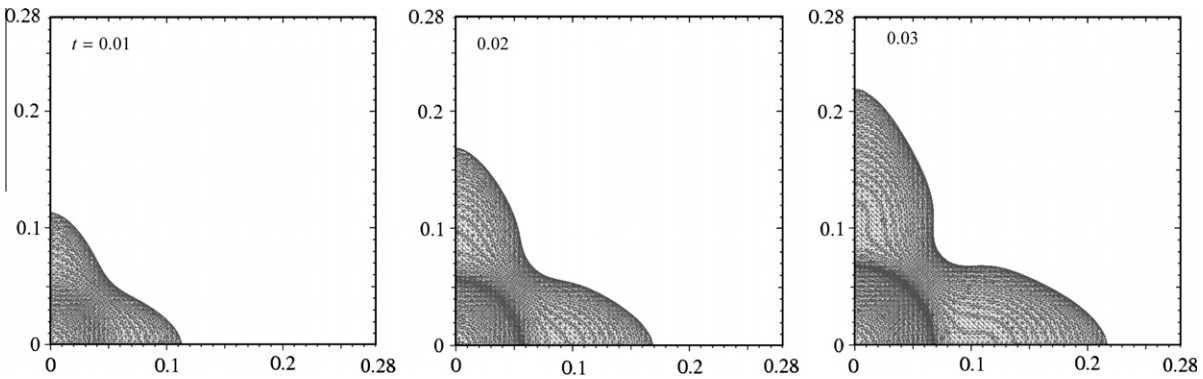

Fig. 6. Dendritic growth simulation test in 3D. Computed results for the interface shape at different instants, using a grid of 120^3 cells. The isocontours of $F = 0.5$, triangulated using the method described in [17], are represented.

Although a finer grid would be necessary to obtain grid-independent results, a comparison between our results for the evolution of the interface shape, shown in Fig. 6, and the results of a front-tracking method presented by Zhao et al. [37], both of them obtained with the same grid size, reveals a good degree of agreement. As in [37], the averaged tip radius was calculated over a time period of 0.01–0.03, yielding a value of 0.0143, which is very close to that of 0.0148 obtained by these authors.

The most time-consuming task in this test is the resolution of the energy equation, even though the Bi-CGSTAB algorithm converges very fast in this type of problem (generally only 7–9 iterations are needed). We found that this task requires a fraction of the total CPU-time of about 80%.

4. Conclusions

A new methodology has been proposed for the simulation of dendritic growth of pure metals, which is based on a VOF method with PLIC reconstruction of the interface and a diffuse-interface method to solve the energy equation. A distance function distribution is used to define the diffuse-interface. The thermal gradients at both sides of the interface are used to accurately obtain the interface velocity. The resolution of the advection equation of a discretized solid fraction function and the calculation of the interface curvature are carried out using accurate methods that have recently been proposed. The numerical results obtained with the proposed model have been compared with analytical solutions and with numerical results obtained by other authors for the formation of complex dendritic structures in two and three dimensions. The good degree of agreement found demonstrates that the volume of fluid method may be considered a good alternative method for the simulation of solidification processes.

Acknowledgments

The authors gratefully acknowledge the support of the Spanish Ministerio de Educación y Ciencia under Grants DPI2006-07047 and DPI2007-63275, and the Spanish Fundación Séneca (Agencia de Ciencia y Tecnología de la Región de Murcia) under Grant 05802/PI/07.

References

[1] V. Alexiades, A.D. Solomon, Mathematical Modeling of Melting and Freezing Processes, Hemisphere, Washington, DC, 1993.
[2] R. Almgren, Variational algorithms and pattern formation in dendritic solidification, J. Comput. Phys. 106 (1993) 337–354.
[3] N. Al-Rawahi, G. Tryggvason, Numerical simulation of dendritic solidification with convection: two-dimension geometry, J. Comput. Phys. 180 (2002) 471–496.
[4] N. Al-Rawahi, G. Tryggvason, Numerical simulation of dendritic solidification with convection: three-dimensional flow, J. Comput. Phys. 194 (2004) 677–696.
[5] C. Beckermann, H.-J. Diepers, I. Steinbach, A. Karma, X. Tong, Modeling melt convection in phase-field simulations of solidification, J. Comput. Phys. 154 (1999) 468–496.
[6] W.J. Boettinger, J.A. Warren, C. Beckermann, A. Karma, Phase-field simulation of solidification, Annu. Rev. Mater. Res. 32 (2002) 163–194.
[7] A. Bourlioux, A coupled level-set volume-of-fluid algorithm for tracking material interfaces, in: Proceedings 6th International Symposium on Computational Fluid Dynamics, 1995, Lake Tahoe, CA, USA.
[8] S. Chen, B. Merriman, S. Osher, P. Smereka, A simple level set method for solving Stefan problems, J. Comput. Phys. 135 (1997) 8–29.
[9] S.J. Cummins, M.M. Francois, D.B. Kothe, Estimating curvature from volume fractions, Comput. Struct. 83 (2005) 425–434.
[10] F. Gibou, R.P. Fedkiw, L.-T. Cheng, M. Kang, A second-order-accurate symmetric discretization of the Poisson equation in irregular domains, J. Comput. Phys. 176 (2002) 205–227.
[11] J. Hernández, J. López, P. Gómez, C. Zanzi, F. Faura, A new volume of fluid method in three dimensions. Part I: Multidimensional advection method with face-matched flux polyhedra, Int. J. Numer. Methods Fluids 58 (2008) 897–921.
[12] A. Jacot, M. Rappaz, A pseudo-front tracking technique for the modelling of solidification microstructures in multi-component alloys, Acta Mater. 50 (2002) 1909–1926.
[13] D. Juric, G. Tryggvason, A front-tracking method for dendritic solidification, J. Comput. Phys. 123 (1996) 127–148.
[14] A. Karma, W.J. Rappel, Quantitative phase-field modelling of dendritic growth in two and three dimensions, Phys. Rev. E 57 (1998) 4323–4349.
[15] Y.-T. Kim, N. Goldenfeld, J. Dantzig, Computation of dendritic microstructures using a level set method, Phys. Rev. E 62 (2000) 2471–2474.
[16] J. López, J. Hernández, P. Gómez, F. Faura, A volume of fluid method based on multidimensional advection and spline interface reconstruction, J. Comput. Phys. 195 (2004) 718–742.
[17] J. López, C. Zanzi, P. Gómez, F. Faura, J. Hernández, A new volume of fluid method in three dimensions. Part II: Piecewise-planar interface reconstruction with cubic-Bézier fit, Int. J. Numer. Methods Fluids 58 (2008) 923–944.
[18] J. López, J. Hernández, Analytical and geometrical tools for 3D volume of fluid methods in general grids, J. Comput. Phys. 227 (2008) 5939–5948.
[19] J. López, C. Zanzi, P. Gómez, R. Zamora, F. Faura, J. Hernández, An improved height function technique for computing interface curvature from volume fractions, Comput. Methods Appl. Mech. Eng. 198 (2009) 2555–2564.
[20] M. Malik, E.S.-C. Fan, M. Bussmann, Adaptive VOF with curvature-based refinement, Int. J. Numer. Methods Fluids 55 (2007) 693–712.
[21] T. Menard, S. Tanguy, S. Berlemont, Coupling level set/VOF/ghost fluid methods: validation and application to 3D simulation of primary break-up of a liquid jet, Int. J. Multiphase Flow 33 (2007) 510–524.
[22] D. Pal, J. Bhattacharya, P. Dutta, S. Chakraborty, An enthalpy model for simulation of dendritic growth, Numer. Heat Transfer B 50 (2006) 59–78.
[23] N. Provatas, N. Goldenfeld, J. Dantzig, Efficient computation of dendritic microstructures using adaptive mesh refinement, Phys. Rev. Lett. 80 (1998) 3308–3311.
[24] Y. Saad, Iterative Methods for Sparse Linear Systems, SIAM, Philadelphia, 2003.
[25] R. Scardovelli, S. Zaleski, Direct numerical simulation of free-surface and interfacial flow, Annu. Rev. Fluid Mech. 31 (1999) 567–603.
[26] J.A. Sethian, J. Straint, Crystal growth and dendritic solidification, J. Comput. Phys. 98 (1992) 231–253.
[27] M. Sussman, E.G. Puckett, A coupled level set and volume-of-fluid method for computing 3D axisymmetric incompressible two-phase flows, J. Comput. Phys. 162 (2000) 301–337.

[28] K.-H. Tacke, A. Harnisch, Finite Difference Enthalpy Methods for Dendritic Growth, Proceedings of the International Conference on Computational Modeling of Free and Moving Boundary Problems, WIT Press, Southampton, 1991.
[29] L. Tan, N. Zabaras, A level set simulation of dendritic solidification with combined features of front-tracking and fixed-domain methods, J. Comput. Phys. 211 (2006) 36–63.
[30] H.S. Udaykumar, R. Mittal, W. Shyy, Computation of solid–liquid phase fronts in the sharp interface limit on fixed grids, J. Comput. Phys. 153 (1999) 535–574.
[31] V.R. Voller, An enthalpy method for modeling dendritic growth in a binary alloy, Int. J. Heat Mass Transfer 51 (2008) 823–834.
[32] J.A. Warren, W.J. Boettinger, Prediction of dendritic growth and microsegregation patterns in a binary alloy using the phase-field method, Acta Mater. 43 (1995) 689–703.
[33] X. Yang, A.J. James, J. Lowengrub, X. Zheng, V. Cristini, An adaptive couple level-set/volume-of-fluid interface capturing method for unstructured triangular grids, J. Comput. Phys. 217 (2007) 364–394.
[34] N. Zabaras, D. Samanta, A stabilized volume-averaging finite element method for flow in porous media and binary alloy solidification processes, Int. J. Numer. Methods. Eng. 60 (2004) 1103–1138.
[35] P. Zhao, J.C. Heinrich, Front-tracking finite element method for dendritic solidification, J. Comput. Phys. 173 (2001) 765–796.
[36] P. Zhao, J.C. Heinrich, Numerical approximation of a thermally driven interface using finite elements, Int. J. Numer. Methods Eng. 56 (2003) 1533–1547.
[37] P. Zhao, J.C. Heinrich, D.R. Poirier, Numerical simulation of crystal growth in three dimensions using a sharp-interface finite element method, Int. J. Numer. Methods Eng. 71 (2007) 25–46.
[38] VOFTools, a package of FORTRAN subroutines with analytical and geometrical tools for 2D/3D VOF methods in general grids <http://www.dimf.upct.es/personal/lrj/voftools.html>.